Obrabotka metallov (tekhnologiya, oborudovanie, instrumenty) = Metal Working and Material Science. 2026 vol. 28 no. 3 pp. 44–57
ISSN: 1994-6309 (print) / 2541-819X (online)
DOI: 10.17212/1994-6309-2026-28.3-44-57

NSTU NETI

Obrabotka metallov - Metal Working and Material Science

Journal homepage: http://journals.nstu.ru/obrabotka_metallov

The influence of laser cladding modes on the defectiveness of Ni-Al coatings

Natalya Kozhukhova [a], *Vyacheslav Sirota* [b, *], *Anton Churikov* [c], *Sergey Zaitsev* [d], *Dmitry Prokhorenkov* [e]

Belgorod State Technological University named after V.G. Shukhov, 46 Kostyukova st., Belgorod, 308012, Russian Federation

[a] https://orcid.org/0000-0002-9380-0968, kozhuhovanata@yandex.ru; [b] https://orcid.org/0000-0003-4634-7109, zmas36@mail.ru;
[c] https://orcid.org/0000-0002-1829-2676, churikov.toni@mail.ru; [d] https://orcid.org/0000-0003-0122-1908, sergey-za@mail.ru;
[e] https://orcid.org/0000-0002-6455-8172, bstu-cvt-sem@yandex.ru

ARTICLE INFO

Article history:
Received: 16 June 2026
Revised: 29 June 2026
Accepted: 11 July 2026
Available online: 15 September 2026

Keywords:
Laser cladding
Ni-Al
Coating

Funding
This research was carried out within the framework of the state assignment of the Ministry of Science and Higher Education of the Russian Federation No. FZWN-2026-0007, titled "Structural and Physical Principles of the Formation of Functional Topocomposite Protective Coatings Based on Multicomponent Alloys for Elements of Tunnel Boring Complexes with a High Degree of Abrasive Wear", for the period 2026–2028. The work was also supported by the Center for High Technologies of Belgorod State Technological University named after V. G. Shukhov.

Acknowledgements
The research was carried out using the equipment of the Center for High Technologies of BSTU named after V. G. Shukhov.

ABSTRACT

Introduction. Laser cladding of powder composites is a promising method for producing heat-resistant coatings. The *Ni–Al* system, capable of forming the strengthening Ni_3Al phase, is of interest for protecting components operating under high-temperature oxidation conditions. However, the process is complicated by the high reactivity of aluminum and the tendency to form oxides and embrittle the structure. The literature lacks systematic recommendations for selecting parameters that ensure a dense, defect-free coating for the *Ni*–15% *Al* composition. ***The purpose of this work*** is to optimize the laser cladding parameters of the *Ni–Al* powder composite according to the criteria of continuity, geometric accuracy, and minimal defectiveness of the deposited bead. **Materials and methods.** Cladding was performed using a fiber laser with a power of 1,500–3,900 W, scanning speed of 20–100 mm/min, and powder feed rate of 24–69 g/min. A total of 40 single-track beads were produced. Quality was assessed by visual inspection, metallography of cross-sections, microhardness testing, energy-dispersive X-ray spectroscopy (*EDS*), and X-ray diffraction (*XRD*) phase analysis. The energy input ***E*** and specific energy input ***G*** were calculated for each mode. **Results and discussion.** The minimum energy input required to form a continuous bead is found to be $E \geq 54$ kJ. The optimal parameter window corresponds to ***E*** = 54–81 kJ at a scanning speed of 20–30 mm/min and a laser power of 1,860–2,700 W. At higher specific energy input, the iron content diffusing from the substrate increases, and the heat-affected zone expands. The microhardness of the coatings reaches 260–290 HV, significantly exceeding that of the initial steel substrate (≈150 HV). At lower ***G*** values, the structure contains the strengthening Ni_3Al phase, while at higher ***G*** values, taenite ($Fe_{0.64}Fe_{0.36}$) becomes the dominant phase. Aluminum oxides are not detected in either case. ***Conclusions.*** Modes with ***E*** = 54–81 kJ and ***G*** = 3.3–5.0 kJ/g are recommended, as they provide a dense, defect-free coating with high hardness and the desired phase composition. Further increase in energy input is inadvisable due to excessive dilution with the substrate material. The obtained results can serve as a basis for developing technological regulations for the application of *Ni–Al* coatings.

For citation: Kozhukhova N.I., Sirota V.V., Churikov A.S., Zaitsev S.V., Prokhorenkov D.S. The influence of laser cladding modes on the defectiveness of Ni-Al coatings. *Obrabotka metallov (tekhnologiya, oborudovanie, instrumenty) = Metal Working and Material Science*, 2026, vol. 28, no. 3, pp. 44–57. DOI: 10.17212/1994-6309-2026-28.3-44-57. (In Russian).

Introduction

Laser cladding of powder materials is an effective method for producing metallic coatings and joints [1–3]. The quality of the formed bead – its continuity, geometric accuracy, and the absence of pores, cracks, and lack of fusion – critically depends on the processing parameters: laser power, scanning speed, powder feed rate, and the position of the focal spot [4–6]. Non-optimal selection of parameters leads to defects such

* *Sirota Vyacheslav V.*, Ph.D. (Physics and Mathematics)
Belgorod State Technological University named after V.G. Shukhov,
46 Kostyukova st.,
308012, Belgorod, Russian Federation
Tel.: +7 904 539-14-08, **e-mail:** zmas36@mail.ru

as lack of fusion at the substrate interface, porosity, undercuts, melt splashing, and uneven scaly surface formation [7–9].

The *Ni–Al* system, in particular the composition with 15 wt.% aluminum, is of interest for creating coatings resistant to high-temperature oxidation. However, its laser cladding process is complicated by the high reactivity of aluminum, its tendency to form refractory oxides (Al_2O_3) and intermetallic phases, which increases the risk of embrittlement and cracking [10–12]. The literature contains data on the cladding of nickel and nickel-aluminum coatings with variations in power [13] and speed, but for the *Ni–Al* composition no systematic recommendations exist for selecting parameters that ensure a dense, defect-free bead based on the analysis of bead appearance and cross-sectional microstructure.

In this regard, it is of particular interest to establish quantitative criteria for assessing the quality of the deposited layer – energy input and specific energy input – that allow predicting not only the geometric parameters of the bead but also the phase composition of the resulting coating. As shown in studies [14, 15] for intermetallic systems, the critical factor is not so much the absolute laser power as the balance between the heat input rate and the residence time of the material in the liquid state. During cladding of *Ni–Al* compositions, this balance determines the degree of iron diffusion from the substrate, which, in turn, affects the stability of the strengthening Ni_3Al phase formation. Excessive energy input promotes excessive mixing of the powder with the base material, reducing the heat-resistant properties of the coating, while insufficient energy input leads to incomplete melting of particles and retention of the dendritic structure of the original powder [16].

Furthermore, recent studies [17–19] emphasize the need for a comprehensive approach to quality assessment: visual inspection of the bead appearance should be supplemented by metallographic analysis of cross-sections and X-ray phase analysis, since even with satisfactory macrostructure, hidden defects – micropores, non-metallic inclusions, and undesirable intermetallic phases that reduce performance characteristics – may remain in the coating [20]. For the *Ni–Al* system, such a comprehensive assessment has not been carried out to date, which complicates the development of technological regulations for industrial applications. Given the high sensitivity of the process to parameter variations, it is necessary not only to determine the region of visually acceptable modes but also to establish the boundaries within which the required phase composition and minimal structural defectiveness are maintained.

Thus, ***the purpose of this work*** is to optimize the laser cladding parameters of the *Ni–Al* powder composite according to the criterion of forming a continuous, uniform bead with minimal porosity and defects.

To achieve this aim, ***the following tasks*** were set:

– to perform microscopic analysis of the initial *Ni–Al* powder (shape, size, particle distribution);

– to produce a series of single-track beads with variation in laser power and scanning speed;

– to evaluate the bead appearance and select samples with the best formation (without undercuts, discontinuities, or excessive spattering) based on visual inspection data;

– to investigate cross-sections of the selected samples by optical microscopy, scanning electron microscopy, and X-ray diffraction analysis;

– to determine the technological window of parameters ensuring a dense, high-quality bead for the *Ni–Al* system.

Methods

The powder material used for cladding was 85% *Ni*–15% *Al* powder (produced by *NPO Tulachermet*, *Tula*, Russian Federation), containing 12–15 wt.% aluminum, with a particle size of 40–100 µm.

Scanning electron microscopy results (Fig. 1) showed that the powder particles had an irregular dendritic shape. Particle size analysis was performed using a laser particle size analyzer (*Analysette 22 NanoTec Plus*, *Fritsch*, Germany). According to the results, the particles had the following parameters: d_{10} = 42.1 µm, d_{50} = 68.8 µm, d_{90} = 97.4 µm.

All experiments were carried out using a *SEKIRUS SFL6000* fiber laser (*SEKIRUS*, 6 kW, China) with a *COX3* (*Halden*) coaxial cladding nozzle and a cooling system, mounted on a *KAWASAKI RS020N AC01*

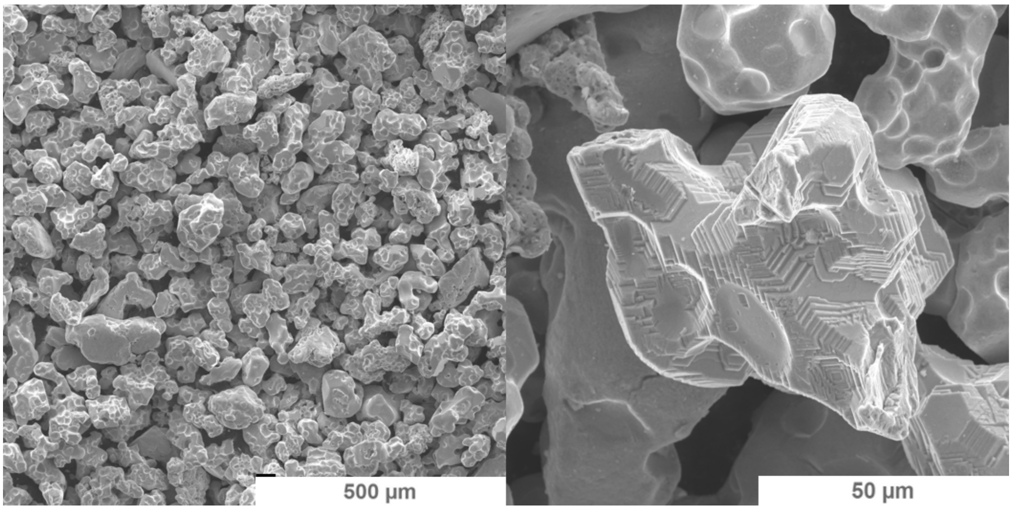

Fig. 1. Appearance of powder 85% *Ni*–15% *Al*

robot (*Kawasaki Heavy Industries*, Japan) with a 5-axis positioner and material feeding via an *ECPF-DCM-D1-2-P2* powder feeder (*Changzhou Xiyu Equipment Co., Ltd.*, China). Argon with a flow rate of 0.4 MPa was used as the carrier gas (Fig. 2).

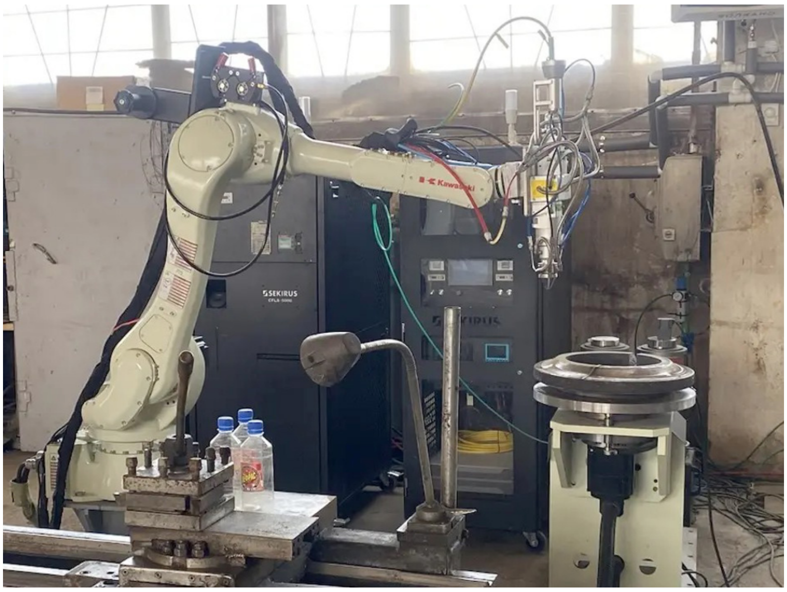

Fig. 2. Appearance of a robotic complex for laser cladding

To optimize the cladding parameters, a series of 40 single-track bead samples 100 mm in length without overlapping was produced. The laser scanning speed $\boldsymbol{V}$ was varied in the range of 20–100 mm/min, the laser power $\boldsymbol{P}$ was varied in the range of 1,500–3,900 W, and the laser spot for cladding on the present device is by default hourglass-shaped; when the focus was set at a distance of 1.5 mm from the substrate, its width was 5 mm and its length 2 mm. The powder feed rate $\boldsymbol{f}$ was in the range of 24–69 g/min. For each 100 mm long bead, the following were calculated: the laser energy input $\boldsymbol{E} = (100/V \times 60) \times P$ and the specific energy input per unit mass $\boldsymbol{G} = E / f \times (100/V)$.

Metallographic specimens were etched in accordance with *ASTM E407*. To reveal the general structure, a solution of acetic acid, HNO_3, and HCl in a volume ratio of 10:10:15 was used. After etching, the cross-sections of single-track beads were subjected to metallographic analysis using an *MT-24RF* optical microscope with *SIAMS 800* software (*SIAMS*, Russia). The microhardness of the cross-section of the cladded coating was measured on a *Nexus 4000* hardness tester using the *Vickers* method at a load of 300 g

(2.942 N) and a dwell time of 15 s. Measurements were performed with a step of 0.12 mm from the coating surface to the substrate. Each hardness value was averaged over three measurements at the same point.

Microstructural studies were carried out on a *Mira 3* scanning electron microscope (*Tescan*, Czech Republic) equipped with an *X-Max 50* energy-dispersive X-ray spectroscopy system with *AZtec* software (*Oxford Instruments*, UK). *SE* and *BSE* images and elemental composition analysis were obtained at an accelerating voltage of 15 kV and a working distance of 15 mm. *EDS* data were processed using *AZtec* specialized software.

The phase composition of the coatings was studied by X-ray diffraction analysis on an *ARL X'TRA* diffractometer with *Co–K*α radiation (λ = 1.790 Å). Measurements were performed in **θ-2θ** scanning mode in the angle range of 10–90° with a step of 0.02° and an exposure time of 1 s per point. Phase identification was carried out using the *PDF-2* database of the *International Centre for Diffraction Data* (*ICDD*).

Results and discussion

It should be noted that the distance from the substrate to the nozzle is determined by the focus of the conical powder stream; in our case, when using the *COX3* nozzle design, this distance was 1.5 mm, so this parameter was not subject to change. During the experiment, 40 single-track bead samples were obtained, each of which was subjected to visual inspection. As a result, four quality categories were identified: non-fused, porous, satisfactory, and good. For the purpose of further analysis and searching for correlation with the calculated values of specific energy input and laser energy input, Fig. 3 presents the bead appearance by category.

The analysis showed that the main criterion determining the presence of defects is the energy input; at ***E*** < 54 kJ, areas of unmelted material were observed in all cases. Beads with excellent visual quality were obtained at ***E*** = 54–81 kJ, which was achieved at a scanning speed of 20–30 mm/min and a laser power of 1,860–2,700 W.

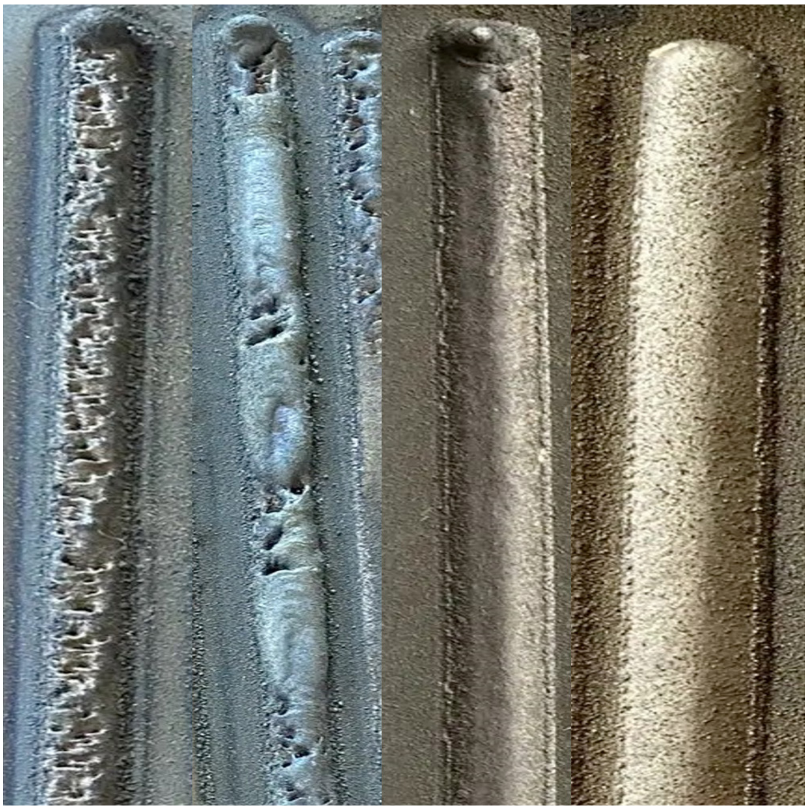

a *b* *c* *d*

Fig. 3. Appearance of roller categories:
a – not fused; *b* – porous; *c* – satisfactory; *d* – good

From the obtained map (Fig. 4), it can be preliminarily concluded that a region within the boundaries of ***E*** = 54–81 kJ and ***G*** = 2–5 contains points with excellent quality. This can be explained by the fact that an increase in the specific energy input, i.e., an increase in excess energy, may disrupt the stability of melting and crystallization processes, which will be discussed in more detail in the analysis of the X-ray diffraction patterns.

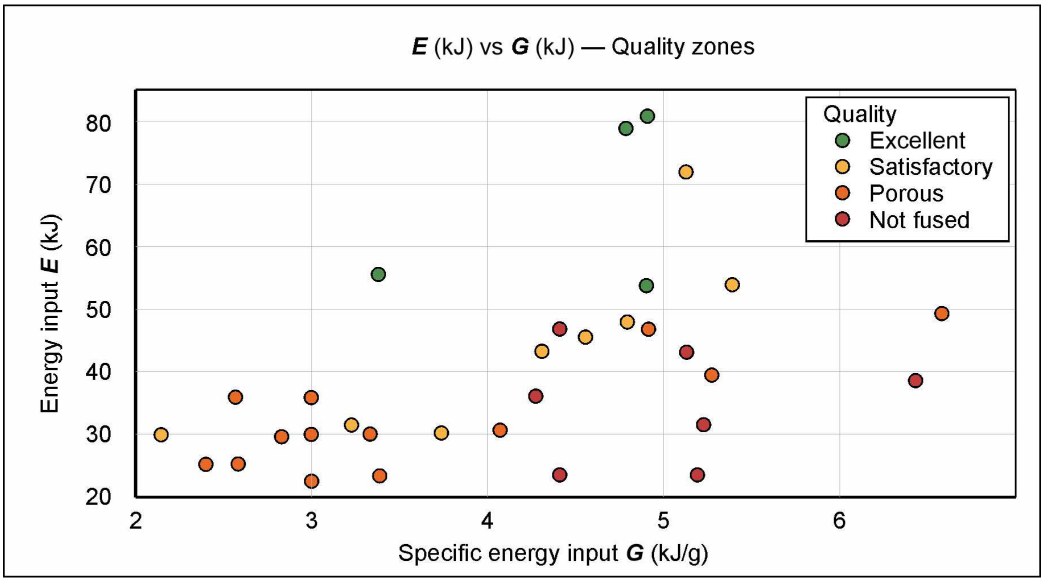

Fig. 4. Quality map in coordinates of energy input ***E*** – specific energy input ***G***

Thus, for further investigation, the most promising are two samples in the identified zone with the minimum and maximum specific energy inputs (Table 1); a comparison of their microstructure and phase composition will confirm the hypothesis about the disruption of crystallization stability with increasing specific energy input in the presented range. For further convenience, the selected samples will be assigned numbers 1 and 2, where sample 1 is the one with a relatively high specific energy input, and sample 2 is the one with the lowest specific energy input from the identified zone, respectively .

Table 1

Selected laser cladding modes

Sample	***V***, mm/min	***P***, W	***E***, kJ	***G***, kJ/g
1	200	2640	79,20	4,91
2	200	1860	55,80	3,38

With the above parameters, the bead quality was optimal both in terms of appearance and hardness characteristics. It is worth noting that the mode for sample 2 corresponds to the lower boundary of the optimal range, while sample 1 corresponds to the upper boundary.

From the presented images (Fig. 5), one can trace the substrate zone that was subjected to thermal effects: in sample 1, this zone extends through the entire thickness of the substrate, while in sample 2 it covers about 80% of the thickness. Pores in the second sample are a recurring problem, because in the cross-section with 4 layers for determining the elemental distribution, such a defect was also detected (Fig. 6), possibly due to insufficient energy closer to the outer boundary of the bead.

It was established that for a single-track bead, an increase in the energy input from 55.8 kJ (sample 2) to 79.2 kJ (sample 1) leads to an increase in the cross-sectional area from 5.5 mm^2 to 7.4 mm^2, which is associated with an increase in the amount of melted material and the depth of substrate penetration. When transitioning to multilayer cladding (three successive beads with overlap), the opposite trend was observed: the total area of the deposited layer was 27.1 mm^2 for sample 1 and 29.6 mm^2 for sample 2. This difference

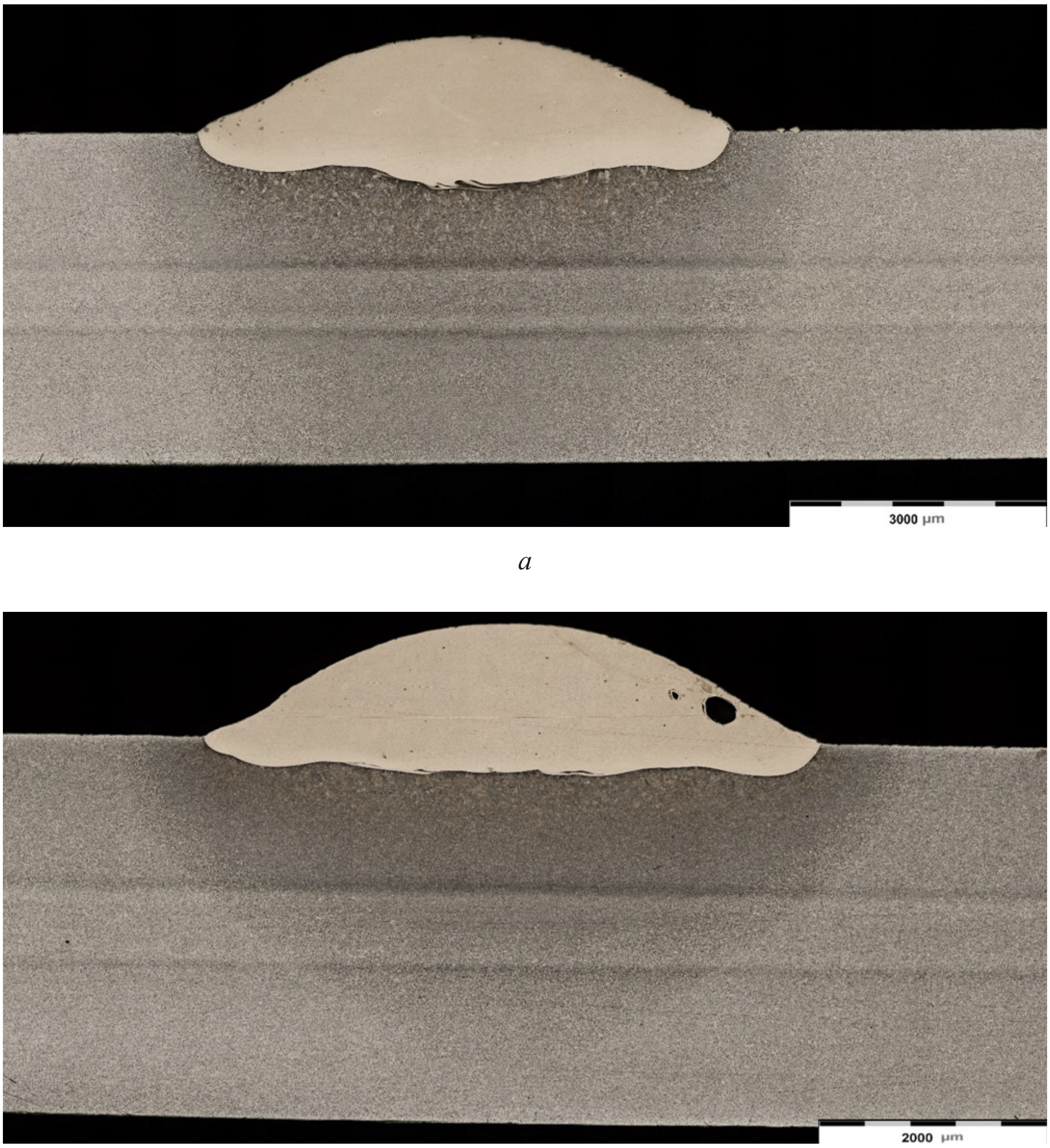

a

b

Fig. 5. Cross-sectional optical micrographs of the obtained samples:
a – sample 1; *b* – sample 2

is explained by the fact that at higher energy input, the proportion of melted and incorporated substrate material increases (which is confirmed by *EDS* data in Fig. 8), but at the same time, the shrinkage of the deposited metal increases due to more intense convection in the melt pool and evaporation of low-melting components. For sample 2 with lower energy input, the melting and crystallization processes proceed more stably, which contributes to the formation of a larger coating volume with a comparable mass of powder fed.

On the hardness graph (Fig. 7), three characteristic zones can be observed: the coating, the buffer zone, and the substrate. It is interesting to note that as a result of laser cladding, the substrate material underwent hardening and its hardness increased by a factor of 1.33 compared to its normal state. Under standard conditions, the hardness of the *St.3* substrate is about 150 HV, and from the graph it can be seen that after the buffer zone, the substrate zone after laser exposure begins, and its hardness is about 200 HV.

The elemental composition profiles were determined using energy-dispersive X-ray spectroscopy of the cross-section from the substrate to the edge of the coating. Fig. 8 presents the results of this work, where the areas of acquisition on the microstructural images are shown first, and below are the elemental distribution graphs.

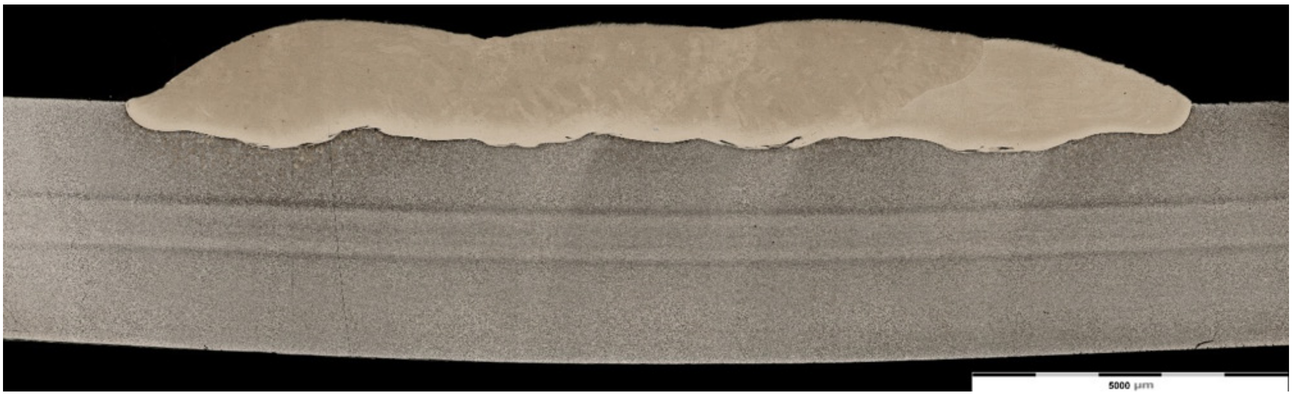

a

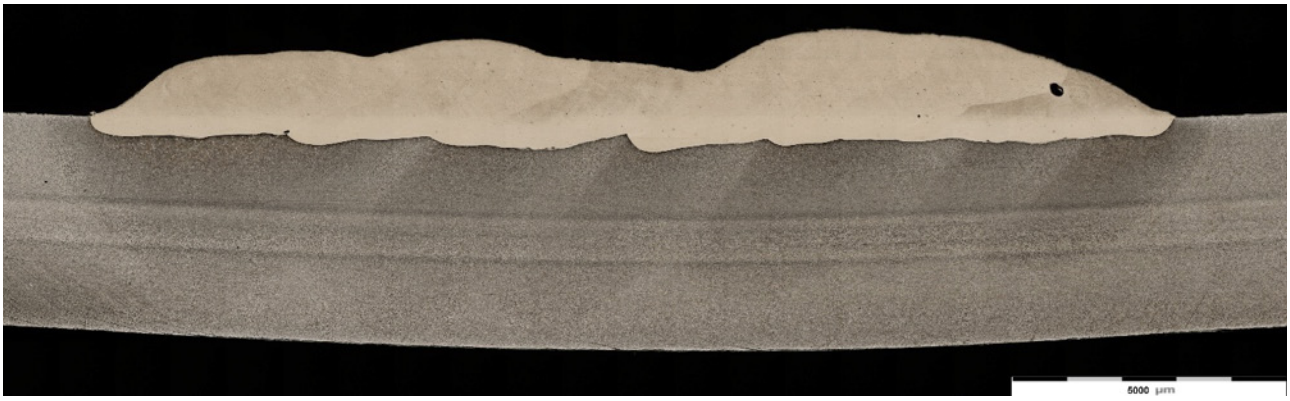

b

Fig. 6. Appearance of the multilayer deposited beads:
a – sample 1; *б* – sample 2

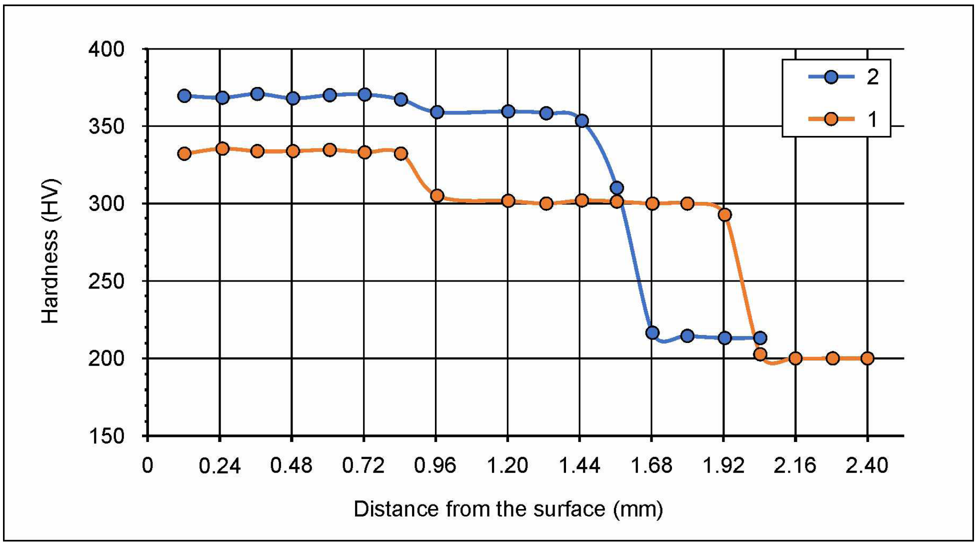

Fig. 7. Hardness of the obtained samples

The analysis of elemental distribution, performed by energy-dispersive X-ray spectroscopy along the scan line from the substrate to the coating surface (Fig. 8), made it possible to establish the nature and degree of diffusion interaction between the deposited material and the base. In both studied samples, complete melting of the surface layer of the substrate and intensive mixing of its material with the Ni–Al powder melt were recorded, as evidenced by the significant iron (Fe) content throughout the coating volume. At the same time, the nature of the elemental distribution differs significantly depending on the energy input.

a

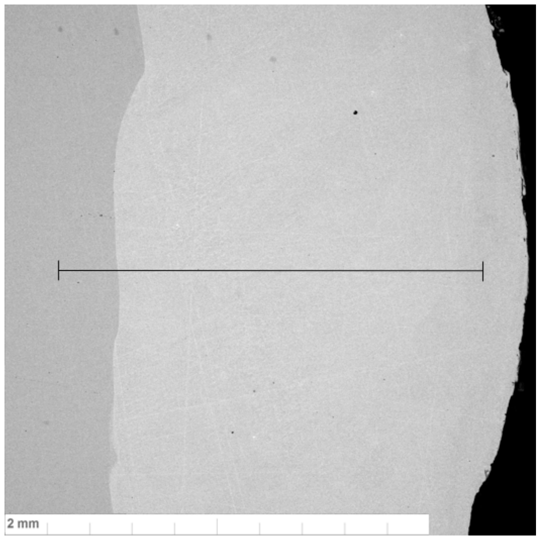

b

c

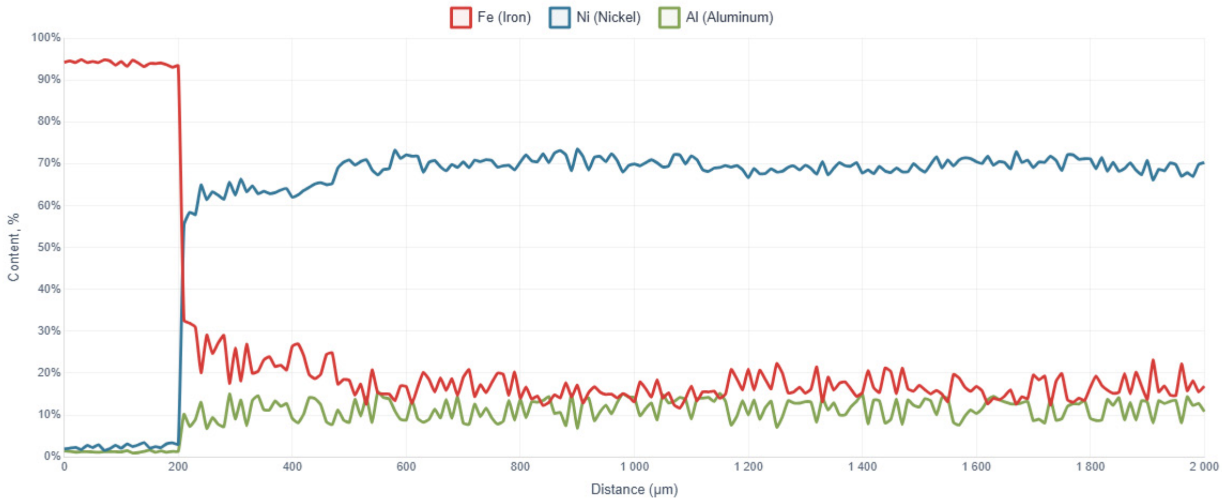

d

Fig. 8. Elemental distribution profiles:

a – microstructure image of sample 1; *b* – microstructure of sample 2; *c* – elemental distribution in sample 1; *d* – elemental distribution in sample 2

For sample 1 (***E*** = 79.2 kJ, ***G*** = 4.91 kJ/g), the average iron concentration in the coating is ≈38–42 wt.%, whereas in sample 2 (***E*** = 55.8 kJ, ***G*** = 3.38 kJ/g) it is ≈28–32 wt.%. The nickel content in the coating naturally decreases with increasing iron impurity fraction: in sample 1 – down to 45–50 wt.%, in sample 2 – down to 55–58 wt.%. The aluminum concentration remains stable at 8–12 wt.% in both cases, which indicates its uniform distribution throughout the melt volume and the absence of segregation, despite its high reactivity. Notably, the iron distribution profile in sample 1 is characterized by a gentler gradient from the substrate to the surface: the Fe concentration decreases from ≈45 wt.% at the interface to ≈35 wt.% in the upper part of the bead, whereas in sample 2 there is a sharp drop from ≈40 wt.% to ≈25 wt.% over the same distance. This indicates more intense convective diffusion in the melt pool at elevated energy input, due to enhanced thermocapillary flow and a longer lifetime of the liquid phase.

With a reduction in the field of view on the scanning electron microscope, the presence and quantity of the formed phases can be examined in more detail.

In sample 1 with higher laser energy input, the formation of three phases was found, one of which has an elongated linear form (Fig. 9, *a*), and two rare phases that can also be observed in sample 2. Based on the shapes, it can be assumed that the denser phase, which appears brighter in the micrographs, is the matrix predominantly consisting of nickel and iron, while the rounded inclusion phase should contain aluminum impurities. The increase in the iron fraction in the coating at high energy input directly correlates with the change in the phase composition, which is confirmed by X-ray diffraction data (Fig. 10). In sample 2 with lower Fe content, a stable intermetallic Ni_3Al phase acting as a strengthener is preserved. In sample 1, on the contrary, excess iron stabilizes the taenite phase ($Fe_{0.64}Ni_{0.36}$), suppressing the formation of Ni_3Al. Thus, an increase in energy input leads not only to geometric changes in the bead but also to an undesirable change in the target phase composition of the coating, which reduces its heat-resistant properties. Consequently, when choosing laser cladding parameters, it is necessary to limit the energy input to values at which iron diffusion does not disrupt the formation of the strengthening intermetallic phase.

The analysis of the X-ray diffraction patterns confirmed the expectation that at lower energy input, the formation of the Ni_3Al phase is more stable, as indicated by the coincidence of the diffraction pattern with the obtained result. Comparison with the microstructure analysis also suggests that during cladding, iron from the substrate mixes with the coating material, and the matrix phase predominantly consists of a non-stoichiometric $Fe_{0.64}Ni_{0.36}$ lattice, while the inclusion phase consists of Ni_3Al. However, analysis of the X-ray diffraction pattern of the second sample showed that the Ni_3Al phase almost ceases to be present

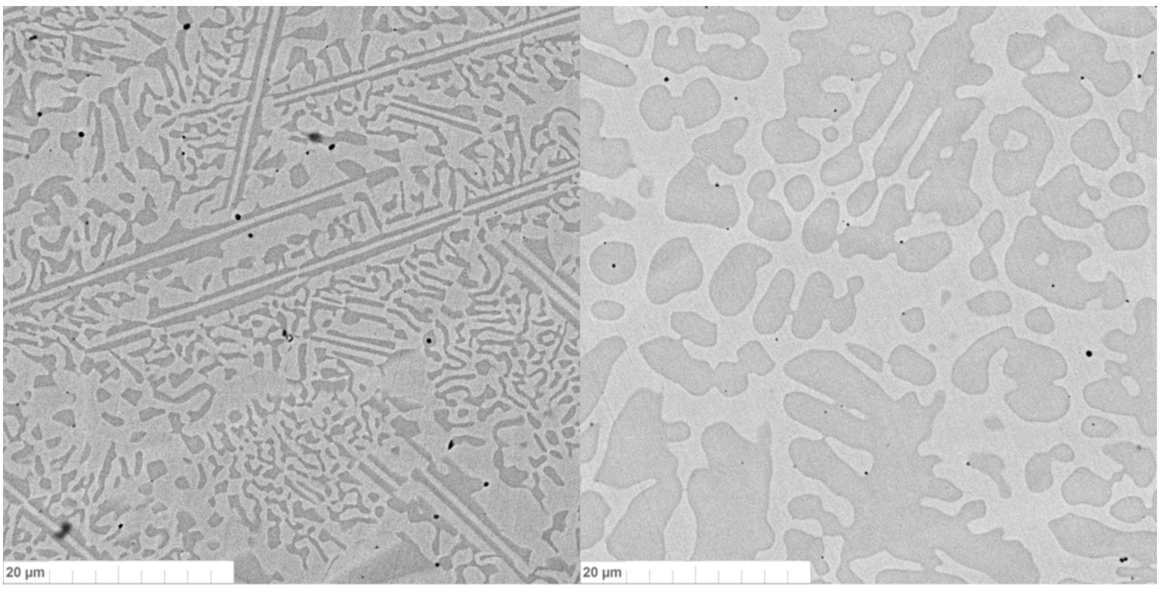

a *b*

Fig. 9. Microstructure of the deposited coatings:
a – sample 1; *b* – sample 2

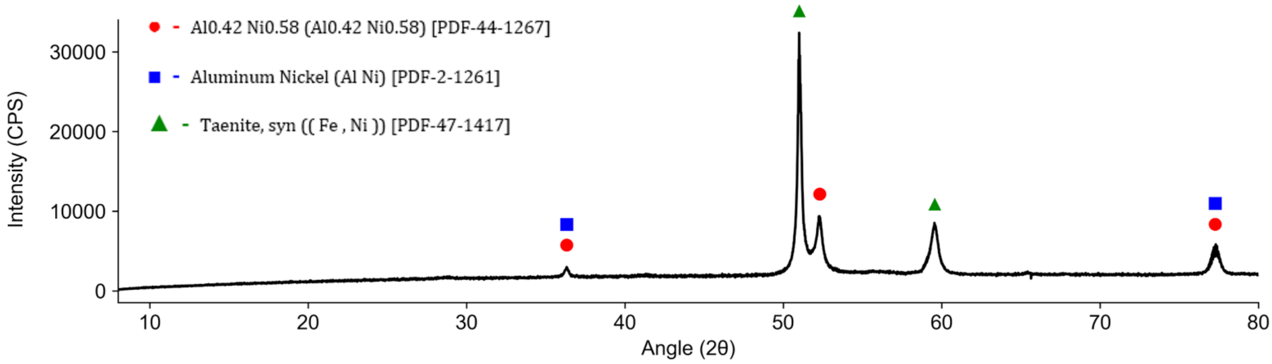

a

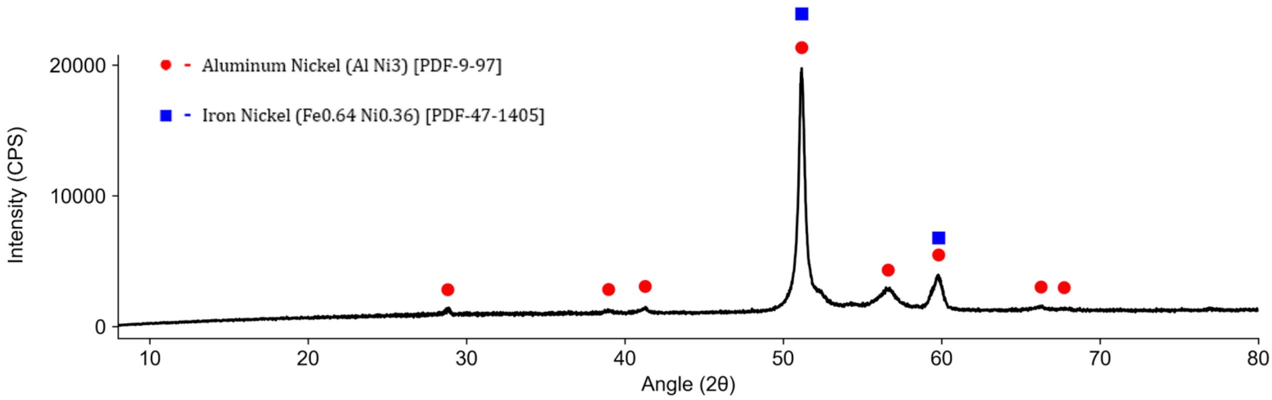

b

Fig. 10. X-ray diffraction patterns of the obtained coatings:
a – sample 1; *b* – sample 2

in the structure, and due to the increased iron content in the coating, the taenite phase is predominantly formed. Notably, no aluminum oxides were detected in the X-ray diffraction patterns, which is also indirectly confirmed by the hardness study, namely its relatively low values.

Conclusion

Based on the results of the conducted experimental studies on laser cladding of the *Ni–Al* powder composite, the regularities of the influence of processing modes on the continuity, defectiveness, and structure of the formed coatings have been established.

The boundaries of energy input determining the bead quality have been established. The minimum energy input required to initiate melting and form a continuous bead is $\boldsymbol{E} \geq 54$ kJ. At $\boldsymbol{E} < 54$ kJ, areas of unmelted material and lack of fusion with the substrate are observed in all cases.

The region of optimal parameters providing a visually high-quality bead without undercuts, discontinuities, and significant spattering has been determined. It corresponds to $\boldsymbol{E} = 54–81$ kJ at a scanning speed of 20–30 mm/min and a laser power of 1,860–2,700 W. Under these conditions, a uniform bead with minimal porosity is formed.

Within the optimal region, two samples with different specific energy inputs ($\boldsymbol{G}$ = 4.91 kJ/g and $\boldsymbol{G}$ = 3.38 kJ/g) were selected. Comparative analysis showed:

– both samples have a dense structure without macrocracks;

– the sample with higher $\boldsymbol{G}$ (sample 1) is characterized by an enlarged heat-affected zone (extending through the entire substrate thickness) and a larger bead cross-sectional area (7.4 mm^2 vs. 5.5 mm^2);

– at higher energy input, the proportion of iron diffusing from the substrate into the coating increases, which changes the phase composition;

– the microhardness of the coatings is at the level of 260–290 HV, which significantly exceeds the hardness of the original St.3 steel (≈150 HV). At the same time, the hardness of the substrate after cladding increases to ≈200 HV due to thermal hardening.

Phase analysis showed that at lower specific energy input (sample 2); the structure is more stable and contains the Ni_3Al strengthening phase. At higher energy input (sample 1), the iron content increases, which leads to the predominant formation of the taenite phase ($Fe_{0.64}Ni_{0.36}$) and a decrease in the proportion of Ni_3Al. It is important to note that in both cases, no aluminum oxides (Al_2O_3) were detected, which indicates effective protection of the melt by argon.

Practical significance. The obtained data allow the following modes to be recommended for the *Ni–Al* system: $\boldsymbol{E}$ = 54–81 kJ and $\boldsymbol{G}$ = 3.3–5.0 kJ/g, as they provide a dense, defect-free coating with high hardness. A further increase in specific energy input is inadvisable, as it leads to excessive dilution with the substrate and changes in the target phase composition.

Thus, the aim of the work – optimization of laser cladding parameters for *Ni–Al* according to the criteria of continuity, geometric accuracy, and minimal defectiveness – has been achieved. The identified parameter window can serve as a basis for developing technological regulations for the application of *Ni–Al* coatings on components operating under high-temperature oxidation conditions.

References

1. Zhong M., Liu W. Laser surface cladding: the state of the art and challenges. *Proceedings of the Institution of Mechanical Engineers, Part C: Journal of Mechanical Engineering Science*, 2010, vol. 224 (5), pp. 1041–1060. DOI: 10.1243/09544062JMES1782.

2. Wang K., Zhang Z., Xiang D., Ju J. Research and progress of laser cladding: process, materials and applications. *Coatings*, 2022, vol. 12 (10), p. 1382. DOI: 10.3390/coatings12101382.

3. Li C. Research progress and prospect of laser cladding technology. *Journal of Physics: Conference Series*, 2023, vol. 2419 (1), p. 012049. DOI: 10.1088/1742-6596/2419/1/012049.

4. Makarov A.M., Gerashchenkov D.A., Kuznetsov P.A., Ryabov V.V., Vasiliev O.S. Investigation of the influence of laser treatment modes on coatings of aluminum, nickel, nickel-titanium systems. *Journal of Physics: Conference Series*, 2021, vol. 1758 (1), p. 012024. DOI: 10.1088/1742-6596/1758/1/012024.

5. Bourahima F., Helbert A.L., Rege M., Ji V., Solas D., Baudin T. Laser cladding of Ni based powder on a Cu-Ni-Al glassmold: Influence of the process parameters on bonding quality and coating geometry. *Journal of Alloys and Compounds*, 2019, vol. 771, pp. 1018–1028. DOI: 10.1016/j.jallcom.2018.09.004.

6. Pang X., Zhao Y., Liu W., He Z. Effect of laser power on the microstructure, wear and corrosion resistance of laser-clad Ni45 nickel-based alloy coatings. *Coatings*, 2026, vol. 16 (2), p. 238. DOI: 10.3390/coatings16020238.

7. Wang Z., Zhang J., Zhang F., Qi C. Study on the microstructure and properties of a laser cladding Fe–Ni–Al coating based on the invar effect. *Scientific Reports*, 2024, vol. 14 (1), p. 11685. DOI: 10.1038/s41598-024-62306-6.

8. Zhang H., He Y., Zhang T., Fu Y., Huang K. Microstructure and wear characteristics of nickel-based coatings produced via laser cladding on 6061 aluminum alloy. *Lubricants*, 2026, vol. 14 (2), p. 56. DOI: 10.3390/lubricants14020056.

9. Haldar B., Saha P. Identifying defects and problems in laser cladding and suggestions of some remedies for the same. *Materials Today: Proceedings*, 2018, vol. 5 (5), pp. 13090–13101. DOI: 10.1016/j.matpr.2018.02.297.

10. Chen M., Yang X., Zhang Z., Gu Y., Li K., Liu Y., Ma J. Research status of laser cladding technology on aluminum alloy surface. *The International Journal of Advanced Manufacturing Technology*, 2025, vol. 137 (1), pp. 1–21. DOI: 10.1007/s00170-025-15204-8.

11. Luis N.C. *Transition metal aluminide coatings and initial steps on additive manufacturing*. London, IntechOpen, 2018. DOI: 10.5772/intechopen.72582.

12. Cheng G.P., He Y.Z. Preparing of NiAl and Ni_3Al intermetallic composite coatings by laser cladding in situ synthesis. *Advanced Materials Research*, 2011, vol. 239, pp. 636–641. DOI: 10.4028/www.scientific.net/AMR.239-242.636.

13. Wang X., Liu Z., Cheng K., Li J., Ning H., Mao J. High-temperature corrosion characterization of Ni–Al laser cladding: the effect of Al content and Fe. *Journal of Thermal Spray Technology*, 2024, vol. 33 (5), pp. 1417–1439. DOI: 10.1007/s11666-024-01782-8.

14. Gulov M.A. Optimizatsiya parametrov lazernoi naplavki poroshka na osnove sistemy nikel'-alyuminii [Optimization of parameters of laser cladding of the powder based on nickel-aluminium system]. *Sibirskii*

fizicheskii zhurnal = Siberian Journal of Physics, 2022, vol. 17, no. 1, pp. 65–77. DOI: 10.25205/2541-9447-2022-17-1-65-77.

15. Kotoban D., Grigoriev S., Shishkovsky I. Study of 3D laser cladding for $Ni_{85}Al_{15}$ superalloy. *Physics Procedia*, 2014, vol. 56, pp. 262–268. DOI: 10.1016/j.phpro.2014.08.170.

16. Wang K., Zhang Z., Xiang D., Ju J. Research and progress of laser cladding: process, materials and applications. *Coatings*, 2022, vol. 12 (10), p. 1382. DOI: 10.3390/coatings12101382.

17. Bourahima F., Helbert A.L., Rege M., Ji V., Solas D., Baudin T. Laser cladding of Ni based powder on a Cu–Ni–Al glassmold: Influence of the process parameters on bonding quality and coating geometry. *Journal of Alloys and Compounds*, 2019, vol. 771, pp. 1018–1028. DOI: 10.1016/j.jallcom.2018.09.004.

18. Moosa A.A., Kadhim M.J., Subhi A.D. Dilution effect during laser cladding of Inconel 617 with Ni–Al powders. *Mathematical Models and Methods in Applied Sciences*, 2011, vol. 5, p. 50.

19. Zhang G., Ren Z., Hou Y., Zheng H. Laser cladding Al/Ni composite coating and its tribology performance. *Surface Engineering*, 2025, vol. 41 (2), pp. 266–278. DOI: 10.1177/02670844241309306.

20. Kotoban D.V., Shishkovsky I.V. Experimental study of conditions for the 3D laser cladding of nickel aluminide. *Bulletin of the Russian Academy of Sciences: Physics*, 2016, vol. 80 (8), pp. 1003–1006. DOI: 10.3103/s1062873816080268. Translated from *Izvestiya Rossiiskoi akademii nauk. Seriya fizicheskaya*, 2016, vol. 80, no. 8, pp. 1101–1105. DOI: 10.7868/S0367676516080263.

Conflicts of Interest

The authors declare no conflict of interest.